ACS APPLIED MATERIALS & INTERFACES

Surfaces, Interfaces, and Applications

Polarization Selectivity of the Thin Metal Film Plasmon-Assisted Fiber-Optic Polarizer

Xinyue Wang, Jintong Lin, Wen Sun, Zhongwei Tan, Rui Liu, and Ziyu Wang

ACS Appl. Mater. Interfaces, **Just Accepted Manuscript** • DOI: 10.1021/acsami.0c08274 • Publication Date (Web): 19 Jun 2020

Polarization Selectivity of the Thin Metal Film Plasmon-Assisted Fiber-Optic Polarizer

Xinyue Wang,[*,†] *Jintong Lin,*[‡] *Wen Sun,*[†] *Zhongwei Tan,*[§] *Rui Liu,*[†] *Ziyu Wang*[*,∥]

[†]College of Information and Electrical Engineering, China Agricultural University, Beijing 100083, China.

[‡]State Key Laboratory of Information Photonics and Optical Communications, Institute of Information Photonics and Optical Communications, Beijing University of Posts and Telecommunications, Beijing 100876, China.

[§]Photonics Research Centre, Department of Electronic and Information Engineering, The Hong Kong Polytechnic University, Hong Kong 999077, China.

[∥]State Key Laboratory of Advanced Optical Communication Systems and Networks, Department of Electronics, Peking University, Beijing 100871, China.

[*]Corresponding author. E-mail: 2014016@cau.edu.cn; wangziyu@pku.edu.cn

ABSTRACT: The interaction between light and metallic nanostructures leads to many impressive achievements and has a wide range of applications. The thin metal film plasmon-assisted fiber-optic polarizer is one of the essential applications. However, the polarization mechanism and the transmitted polarization of the plasmon-assisted polarizer have existed controversy over the past decade. Which one of the polarizations is preferentially transmitted through the polarizer? The transverse electric polarization or the transverse magnetic polarization? Here, special emphasis is placed upon the polarization mechanism and the transmitted polarization of thin metal film plasmon-assisted fiber polarizers. We first investigate the polarization mechanism of the polarizers theoretically and numerically. Furthermore, a novel approach is proposed to demonstrate the transmitted polarization in the plasmon-assisted fiber polarizers experimentally. We demonstrate that the polarization mechanism is based on the polarization selective absorption of the metallic material, and the transverse electric polarization is the only transmitted polarization of the metallic plasmon-assisted polarizer. Moreover, the plasmon-assisted polarizer can offer a high polarization extinction ratio (33.1dB) and a low insertion loss (1.1dB) at room temperature and have an excellent temperature stability in the range of -48~82°C. Experimental results agree well with our theoretical and numerical analysis. The findings clarify the confusion about the polarization mechanism and the transmitted polarization of metallic plasmon-assisted fiber polarizers over the past decade, providing new ground for the exploration of polarization sensitive optical systems, with a good potential applications in the fields of optical sensors, plasmonic lasers, coherent optical communications, as well as biosensor systems.

KEYWORDS: metallic material, plasmonic devices, metal-dielectric interface, polarization of light, optical polarizers

INTRODUCTION

For decades, metallic materials were regarded as dull and useless for optical devices.[1] In recent years, however, the interaction between light and metallic nanostructures leads to many impressive achievements that propel plasmonic optics to a very lively and productive research area.[2-4] With the development of accurate and reliable nanofabrication techniques, metals bridge the gap between classical optics and plasmonic optics, and have a wide range of applications.[5-10] The thin metal film plasmon-assisted fiber-optic polarizer is one of the essential applications. Polarizers are very important devices for polarization filtering and analyzing. Many optical systems have operational characteristics that are highly dependent on the polarization of the light, including biosensors, interferometric sensors, nanowire lasers, coherent optical communications, and quantum communications, etc.[11-15] Many types of polarizers with different structures or different polarization mechanisms, such as birefringence, reflection, selective absorption, and scattering, have been reported.[16,17] Initially, attention has focused on bulk-optic polarizers.[16] With the discovery and exploration of surface plasmon polaritons (SPPs)[18-20] and the development of accurate and dependable nano-fabrication techniques,[21-25] fiber polarizers, including metallic plasmon-assisted fiber polarizers,[26-30] graphene-clad fiber polarizers,[31-33] and plasmonic photonic crystal fiber polarizers blossomed.[34,35]

It is easy to clarify the polarization mechanism and to figure out the transmitted polarization of the bulk-optic polarizer. There are, however, two opinions regarding the transmitted polarization of the metallic plasmon-assisted polarizer, the transverse electric (TE) polarization (electric field parallel to the metal plane) or the transverse magnetic (TM) polarization (electric field perpendicular to the metal plane). Some studies have reported the transmitted polarization of the polarizer to be TE polarization,[36-38] while others came to a different conclusion.[31,39,40] For example, in their *Nature Photonics* letter,[31] Bao et al. only observed a TM pass polarizing effect in metal-clad plasmon-assisted fiber polarizers. In an *Electronics Letter*, Eickhoff[40] claimed that there were two possible ways of making TE or TM pass polarizers in such a structure. However, all these conclusions were drawn from theoretical predictions or unprecise experimentation (1. Using single-mode (SM) fibers to fabricate the optical fiber polarizer and in their systems.[31,40] As is known to all, polarization properties of SM fibers are easily disturbed by environmental factors. 2. Investigating the state of polarization (SOP) of the radiated light[31,39] to conjecture the SOP of transmitted light.). It is therefore essential to analyze the polarization state of the light propagating in metallic plasmon-assisted polarizers theoretically and experimentally, in order to clarify the confusion about the polarization mechanism.

Here, special emphasis is placed upon the polarization mechanism and the transmitted polarization of thin metal film plasmon-assisted polarizers instead of only the attenuation differences of the TM and TE polarizations. The polarization mechanism of the metallic plasmon-assisted polarizer is base on the polarization selective absorption of the metallic materials, instead of the radiative loss of the optical fiber, according to the theoretical and simulated results. Furthermore, a novel approach is proposed to demonstrate the transmitted polarization of plasmon-assisted fiber polarizers experimentally. The experimental results conform with the theoretical and numerical analysis, suggesting that the TE mode is the only transmitted polarization of the metallic plasmon-assisted fiber polarizer. Moreover, the plasmon-assisted polarizer can offer a high polarization extinction ratio (PER) of 33.1dB and a low insertion loss (IL) of 1.1dB at room temperature. Compared with the traditional bulk-optic polarizer, the plasmon-assisted polarizer has a more compact and robust configuration and a higher temperature stability with a good potential in applications.

RESULTS AND DISCUSSION

Theory of the metallic plasmon-assisted polarizer. Theoretical analysis of the metallic plasmon-assisted fiber polarizer is based on the theory of the asymmetric metal dielectric multilayer slab waveguide [41,42] (see the Supporting Information for details). Figure 1a,b show the schematic diagrams of the plasmon-assisted fiber polarizer and the two-dimensional (2D) theoretical model, respectively. In this model, the guided wave propagates along the *z*-axis, and the metal plane is perpendicular to the *x*-axis. The electric field can be written as $E(x)\exp[j(\omega t-\beta z)]$, where $\beta = \beta' - j\beta''$ denotes the complex propagation constant along the *z*-axis, β' denotes the phase constant, and β'' denotes the attenuation constant. The propagation losses of the optical waveguide are proportional to β''. The field components for TE modes are E_y, H_x and H_z, and for TM modes are E_x, E_z and H_y. The mode characteristics are determined by applying the boundary conditions, and the complex propagation constants are obtained as the solutions of the eigenvalue equations Eqs. (1)-(6).

$$\kappa_1 d = m\pi + arctan\left(\gamma_{10}\frac{p_0}{\kappa_1}\right) + arctan\left(\gamma_{12}\frac{p_2'}{\kappa_1}\right), m = 0,1,2,3 \ldots \tag{1}$$

$$p_2' = p_2 tan\,h\left[arctanh\left(\gamma_{23}\frac{p_3}{p_2}\right) + p_2 h\right] \tag{2}$$

$$p_0^2 = \beta^2 - k_0^2 n_0^2 \tag{3}$$

$$\kappa_1^2 = k_0^2 n_1^2 - \beta^2 \tag{4}$$

$$p_2^2 = \beta^2 - k_0^2 n_2^2 \tag{5}$$

$$p_3^2 = \beta^2 - k_0^2 n_3^2 \tag{6}$$

Where n_1, n_2 (n_0=n_2) and n_3 are refractive indexes of the core, the cladding and the metal, respectively, p_0, p_2, p_3 and κ_1 are transverse wavenumbers along the *x*-axis in each region, k_0 =

2π/λ is the wavenumber in a vacuum, *d* denotes the diameter of the core, and *h* denotes the buffer layer thickness, as shown in Figure 1b. For TE modes, $\gamma_{10} = \gamma_{12} = \gamma_{23} = 1$, and for TM modes, $\gamma_{10} = \frac{\varepsilon_1}{\varepsilon_0}, \gamma_{12} = \frac{\varepsilon_1}{\varepsilon_2}, \gamma_{23} = \frac{\varepsilon_2}{\varepsilon_3}$, where ε_i is the dielectric constant of each region (*i*=0,1,2,3). The complex dielectric constant of the metal can be written as $\varepsilon_3 = n_3^2 = \varepsilon_3' + j\varepsilon_3''$.

Figure 1c,d show the numerical calculation results of the phase constant β' and the attenuation constant β'' of the first few TE and TM modes as functions of *d*, respectively. The fundamental mode, TM_0, whose electric field is perpendicular to the metal plane, exhibits the behavior of a SPP. It is present because the real part of the dielectric constant of the metal is negative. TM_0 mode differs from the higher order TM mode as well as all TE modes, displaying some special properties.

As shown in Figure 1c, the phase constant β' of TM_0 mode is not constrained to lie between k_0n_2 and k_0n_1, it satisfies $real\left(k_0\sqrt{\frac{\varepsilon_2\varepsilon_3}{\varepsilon_2+\varepsilon_3}}\right) < \beta'_{TM_0} < real\left(k_0\sqrt{\frac{\varepsilon_1\varepsilon_3}{\varepsilon_1+\varepsilon_3}}\right)$, unlike the case of the common guided wave. The TM_0 mode has no cutoff. However, the higher order TM modes and all TE modes have cutoff, for example, the TE_0 mode (red solid line) can only propagate when *d* is larger than 1.35μm.

Figure 1d reveals that the attenuation constants β'' of all TE modes are lower than those of TM modes of the same order. For example, when *d*=3.5μm, only 3 modes can exist, the TM_0 (β''=93060/m), the TM_1 (β''=2030/m) and the TE_0 (β''=47/m) mode. The attenuation constants of the TM_0 and TM_1 modes are much larger than that of the TE_0 mode, especially the SPP mode, TM_0 mode. With the same propagation distance along the *z* direction, the losses of TM modes are much larger than TE modes. It means that for the metallic plasmon-assisted fiber-optic polarizer, the polarization mechanism is based on the differences of the attenuation of the TE and TM polarizations. Therefore, TE polarization is the transmitted polarization of the metallic plasmon-assisted polarizer.

The PER and the IL (the loss of the transmitted polarization) of the metallic plasmon-assisted polarizer can be represented as:

$$\mathrm{PER(dB)} = 10\lg[\frac{P_{TE}}{P_{TM}}] = 10\lg[\frac{\exp(-2\beta''_{TE}L)}{\exp(-2\beta''_{TM}L)}] = \frac{10}{ln10}(2\beta''_{TM} - 2\beta''_{TE})L \qquad (7)$$

$$\mathrm{IL(dB)} = 10\lg[\frac{P_{TE-in}}{P_{TE-out}}] = 10\lg[\frac{1}{\exp(-2\beta''_{TE}L)}] = \frac{10}{ln10}(2\beta''_{TE}L) \qquad (8)$$

Where P_{TE} and P_{TM} are the powers of TE and TM polarizations, respectively, β''_{TE} and β''_{TM} are the attenuation constants of the TE and TM polarizations, respectively, and L is the length of the metal film. The PER (dB) is proportional to the difference of the attenuation constants of the TE and TM modes. IL (dB) is proportional to the attenuation constant of the TE mode (transmitted polarization). PER (dB) and IL (dB) are both proportional to the length of the metal film L.

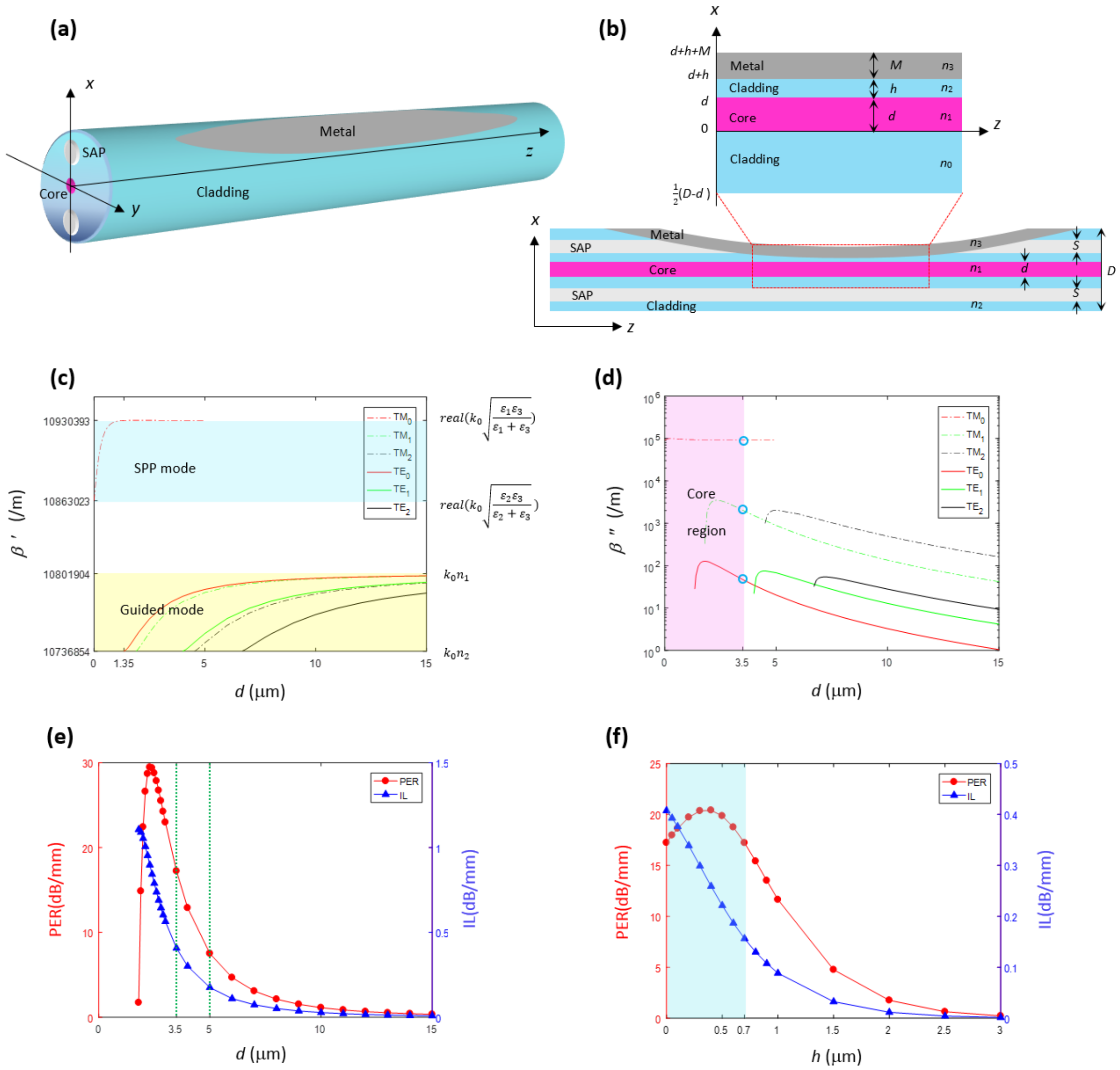

Figure 1. Schematic diagrams and theoretical results of the metallic plasmon-assisted fiber polarizer. (a) Schematic diagram of the plasmon-assisted fiber polarizers. (b) The 2D theoretical model. The diameters of the fiber cladding, the fiber core and the stress applying part (SAP) are D, d and S, respectively. The thicknesses of the metal film and the buffer layer are M and h, respectively. An overview of parameters used in the model is provided in Supporting Table S1. (c) Variation of the phase constant β' with respect to d, (h=0). Solid lines indicate TE modes, and dotted lines indicate TM modes. (d) Variation of the attenuation constant β'' with respect to d, (h=0). (e) PER and IL as functions of d, (h=0). (f) PER and IL as functions of h, (d=3.5μm).

The relationships between the PER, the IL and the fiber core *d* is shown in Figure 1e with *h*=0, according to Eqs. (1)-(8). The red line and the left *y*-axis denote the PER per millimeter metal film, and the blue line and the right *y*-axis are the IL per millimeter metal film. The PER of 7.52 dB/mm and IL of 0.18 dB/mm can be obtained with *d*=5μm (corresponding to Fujikura SM85-PS-U25A, PANDA polarization maintaining (PM) fiber). The PER of 17.23 dB/mm and IL of 0.41 dB/mm can be obtained with *d*=3.5μm (corresponding to Nufern PM850G, PANDA PM fiber which we used in the experimentation).

Figure 1f illustrates the relationships between the PER, the IL and the buffer layer thickness *h* when *d*=3.5μm, according to Eqs. (1)-(8). The red line and the left y-axis denote the PER per millimeter metal film, and the blue line and the right y-axis are the IL per millimeter metal film. The maximum output PER is 20.41 dB/mm with a buffer layer thickness *h*=0.4μm. The maximum IL is 0.41dB/mm with a buffer layer thickness *h*=0μm, and the IL will decrease with the increased of the thickness *h*. Controlling the buffer layer thickness *h*=0-0.7μm will afford a high output PER (17.21-20.41dB/mm) and an acceptable IL (0.16-0.41dB/mm).

Simulations by the FDTD method. With the finite-difference time-domain (FDTD) simulations, we obtain the electric field and the mode field distributions of the metallic thin film plasmon-assisted fiber polarizer, as shown in Figure 2. The SPP mode (TM polarization) appears at the interface of the metallic nano-film and the fiber polished surface as indicated in Figure 2b,d. However, the electric field of TE modes maximizes inside the fiber core as shown in Figure 2c,e. When the polished surface is tangent to the fiber core (as shown in Figure 2), the absorbed power due to the metallic absorption of TM modes is larger than TE modes. With the propagation distance of 20μm, the absorbed power of TM modes is 23.41% of the incident light, while the absorption of TE modes is only 0.97%. When the polished surface reaches the center of the fiber core (see

Supporting Figure S3), the metallic absorptions of both TM and TE modes increase. With the propagation distance of 20μm, the absorbed power of TM modes is 51.16% of the incident light, while the absorption of TE modes is only 2.92%. The propagation losses of TM modes are therefore extremely larger than TE modes.

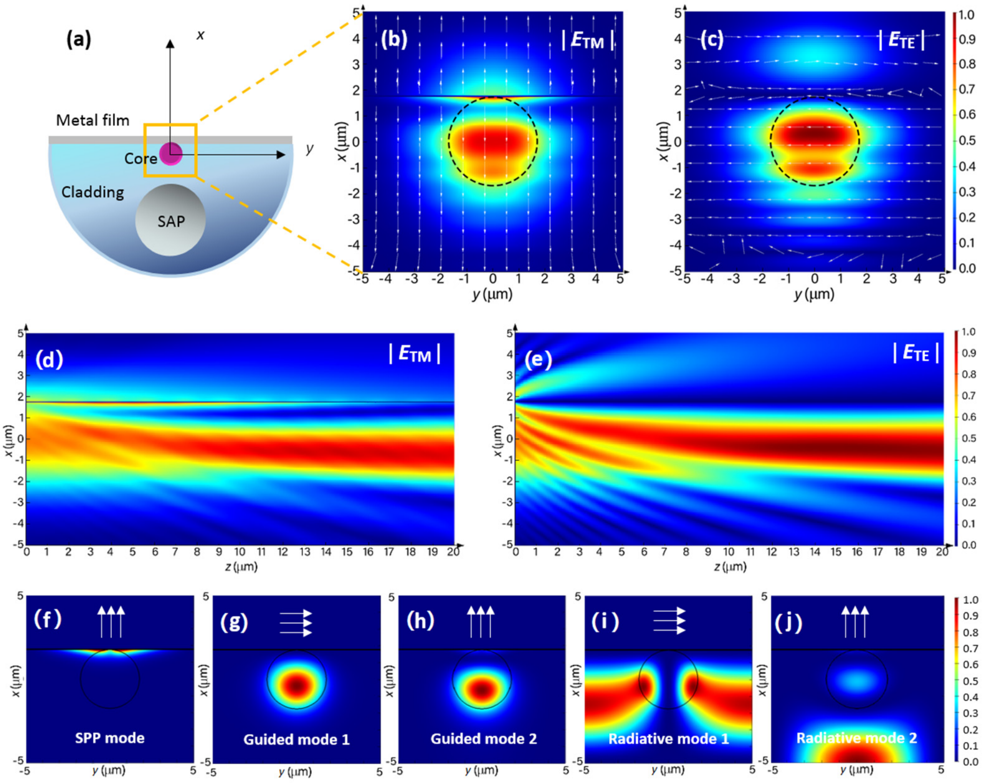

Figure 2. Electric field and mode field distributions of TM and TE modes. (a)Cross section of the plasmon-assisted fiber polarizer. (b),(c)Cross-sectional electric field distributions of TM and TE modes (z=5μm). The electric field amplitudes are normalized to the maximum of TE mode. White arrows represent the polarization orientations of the light. Black dotted circles represent the fiber core regions. (d),(e)Electric field distributions of TM and TE modes in the x-z plane at y=0. Electric field amplitudes are normalized to the maximum of TE mode. (f)-(j)Mode field distributions of the plasmon-assisted polarizer, and the losses of the modes are 832.14dB/mm, 0.39dB/mm,

16.79dB/mm, 3.84dB/mm, 13.3dB/mm, respectively. (f),(h),(j) are TM polarized, and (g),(i) are TE polarized.

Figure 2f-j show the mode field distributions of the metallic plasmon-assisted fiber polarizer. According to mode analysis, the losses of the modes (f)-(j) are 832.14dB/mm, 0.39dB/mm, 16.79dB/mm, 3.84dB/mm, 13.3dB/mm, respectively. The absolute attenuation of TM modes is extremely high for practical implementations.[43,44] Metal losses of TM modes have inhibited the realization of TM pass plasmon-assisted fiber polarizer. This conforms with our theoretical results. The polarization mechanism is based on polarization selective absorption of the metallic materials, and the TE mode is the only transmitted polarization in the metallic plasmon-assisted fiber polarizer. The SPP mode decays very quickly, as shown in Figure 2d, and the radiative modes are evanescent or leaky and have very short propagation lengths. The guided modes, Figure 2g,h, therefore dominate the IL and the PER of the device. The IL and PER of the plasmon-assisted polarizer are 0.39 dB/mm and 16.40 dB/mm, according to FDTD simulations. The simulated results agree well with our theoretical analysis (Figure 1e,f).

Experimentation and discussion. We fabricated a batch of metallic nano-film plasmon-assisted polarizers (see Supporting Information for details) in order to investigate the polarization mechanism, the transmitted polarization, the PER and the IL of the polarizers experimentally. Since the SOP of the SM fiber is easily disturbed by environmental factors[45], we use the PM fiber to fabricate the plasmon-assisted fiber polarizer. Figure 3 shows the scanning electron microscope (SEM, FEI Quanta 600 FEG) images of cross-sections of the plasmon-assisted PM fiber-optic polarizer.

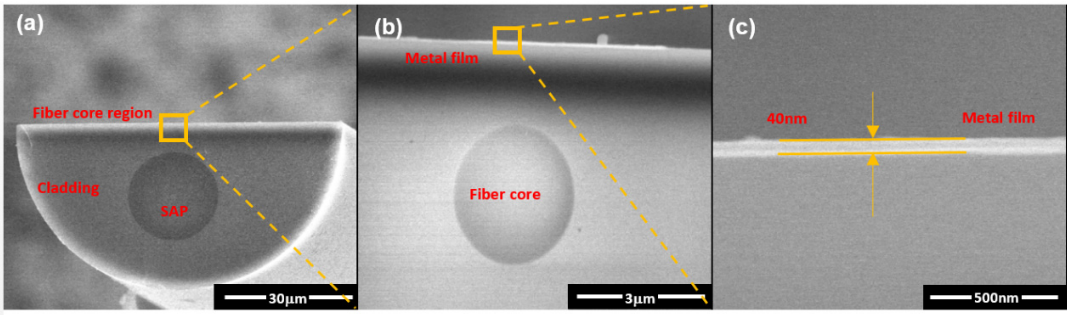

Figure 3. SEM images of the plasmon-assisted polarizer. (a)Cross-sectional image of the plasmon-assisted polarizer. The polished surface is perpendicular to the slow axis of the fiber. The diameters of the fiber cladding, the core and the SAP are about 80μm, 3.5μm, and 21μm, respectively. (b)Cross-sectional image with a different microscope magnification near the fiber core region. The polished surface reaches the evanescent field, and the fiber core is not destroyed. (c)The metallic nano-film is 40 nm thick.

Figure 4a is the experimental set-up for the determination of the transmitted polarization of plasmon-assisted fiber polarizers. To determine which one of the polarizations is preferentially transmitted exactly, the SOP of the transmitted light emerging from the polarization region must be analyzed directly, by cutting samples in half from the region of where the metal film is deposited, instead of evaluating the SOP of radiated light as refs. 31 and 39. Note that all fibers in the experimental set-up are PM fibers to make sure that the SOP is environmentally stable. The partially polarized light from a superluminescent light emitting diode (EXALOS EXS210027, center wavelength 835.90nm, 3dB bandwidth 50.80nm) is launched into the plasmon-assisted fiber-optic polarizer. The plasmon-assisted polarizer is placed in a holder, keeping the metal plane parallel with the *y-z* plane as shown in Figure 4a. The SOP of the transmitted light of the plasmon-assisted fiber-optic polarizer can be analyzed by birefringent polarizers, such as Glan-Taylor(GT) prism. The yellow arrow indicates the transmission axis of the GT prism as shown in the Figure 4a. The polarization parallel with the transmission axis will be transmitted by the GT prism practically unaffected. The transmitted light is detected by the optical detector before it reaches the power meter. When the GT prism is rotated, there is a maximum transmitted power (P_{max}) recorded by the power meter, and a minimum transmitted power (P_{min}) perpendicular to this direction.

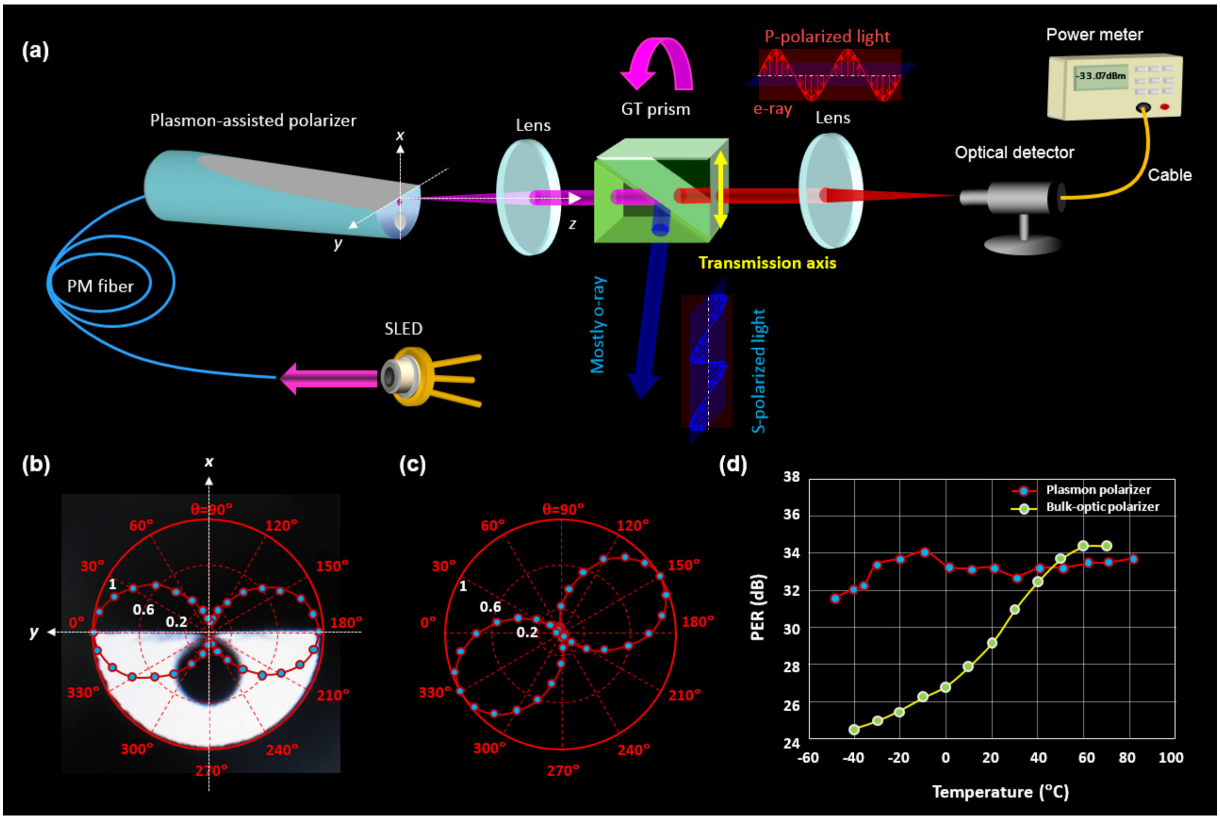

Figure 4. Experimental results. (a) Experimental set-up used to figure out the transmitted polarization of the plasmon-assisted polarizer. The plasmon-assisted polarizer is placed in a holder, keeping the metal plane parallel with the *y*-*z* plane. The GT prism is made of two right-angled prisms of calcite separated on their long faces with an air gap. (b) Polar image of the normalized optical power emerging from the D-shaped cross-section as a function of θ. (c) Polar image of the normalized output optical power of the plasmon-assisted polarizer. (d) PER temperature stability of the plasmon-assisted fiber polarizer compared with the bulk-optic polarizer.

Figure 4b indicates the polar image of the normalized optical power emerging from the D-shaped cross-section as a function of θ. θ denotes the angle between the transmission axis of the GT prism and the *y*-axis. The GT prism is rotated in steps of 10°, and the transmitted power is recorded for each rotation of the prism. When the angle between the *y*-axis and the transmission axis of the GT prism is 90 degrees (θ=90°), the transmitted power is at a minimum (P_{min}= −33.07dBm). It means that the field component transmitted by the cut plasmon-assisted polarizer is perpendicular to the transmission axis of the GT prism. Whereas maximum power, P_{max} = −22.63dBm, occurs when the GT prism is rotated about the *z*-axis through 90 degrees (θ=0°). In this case, the transmission axis of the GT prism and the electric field vector transmitted by the cut plasmon-assisted fiber polarizer are parallel.

Experimental results show that the transmitted power of TM modes is minimal whereas the transmitted power of TE modes is maximal. We determine experimentally that the electric field passed through the metallic plasmon-assisted polarizer is parallel with the metal plane, and the only transmitted polarization of the plasmon-assisted polarizer is the TE polarization. This is very important for the design of polarization sensitive fiber systems and PM fiber devices.

The experimental set-ups used to measure the output PER and the IL of the plasmon-assisted fiber polarizer are shown in Supporting Figures S5 and S6. Figure 4c shows the polar image of the normalized optical power of the plasmon-assisted polarizer. The PER of the tested plasmon-assisted fiber polarizer is 33.1dB and the IL is 1.1dB at room temperature (see Supporting Information for details). Experimental results agree well with our theoretical analysis and simulation results. Figure 4d shows the PER temperature stability of the plasmon-assisted fiber polarizer compared with a traditional bulk-optic polarizer. The PER of the plasmon-assisted fiber polarizer is over 31 dB and the absolute offset is less than 2.5dB in the range of -48~82°C. While the PER offset of the bulk-optic polarizer is more than 10dB in the range of -40~70°C. The performance comparison between the proposed plasmon-assisted fiber polarizer and the previous reports is shown in Table 1. The proposed plasmon-assisted fiber polarizers can offer a high PER (33.1dB) and a low IL (1.1dB) at room temperature, and have an excellent temperature stability in the range of -48~82°C. The proposed plasmon-assisted polarizer has a compact and robust configuration and a high temperature stability with a good potential in applications.

Table 1. Performance Comparison with the Previous Reports

categories	PER(dB) at room temperature	PER(dB) temperature stability	IL(dB) at room temperature	fibers	references
plasmonic fiber polarizer	33.1①	Figure 4d①	1.1①	PM fiber	this work
bulk-optic polarizer	29.1①	Figure 4d①	1.5①	/	this work
plasmonic fiber polarizer	25-30①	not available	1-2①	SM fiber	ref. 28
plasmonic fiber polarizer	27①	not available	7①	SM fiber	ref. 29
integrated plasmonic polarizer	20 / 20②	not available	1 / 0.0635②	/	ref. 30
graphene fiber polarizer	27①	not available	5①	SM fiber	ref. 31
graphene fiber polarizer	25.1 / 26.0②	not available	1.2 / 1.1②	surface core fiber	ref. 32
graphene fiber polarizer	27①	not available	5①	SM fiber	ref. 33

① experimental result ② numerical result

CONCLUSIONS

We demonstrate the polarization mechanism and the transmitted polarization of the metallic nano-film plasmon-assisted fiber polarizer theoretically and experimentally, and clarify that the polarization mechanism is based on the polarization selective absorption of the metal material, and the TE mode is the only transmitted polarization of the metallic plasmon-assisted polarizer. Our findings clarify the confusion about the polarization mechanism and the transmitted polarization of metallic plasmon-assisted fiber polarizers over the past decade. Moreover, the plasmon-assisted fiber polarizers can offer a high PER (33.1dB) and a low IL (1.1dB) at room temperature and have an excellent temperature stability in the range of -48~82°C. The work provides new ground for the exploration of polarization sensitive optical systems, and has a good potential applications in the fields of optical sensors, plasmonic optics, coherent optical communications, as well as biosensor systems.

ASSOCIATED CONTENT

Supporting Information. Additional theoretical analysis of the thin metal film plasmon-assisted polarizers, electric field distributions by the FDTD analysis, details of sample fabrication, and supporting experimental set-ups and results. (PDF)

AUTHOR INFORMATION

Corresponding Author

*E-mail: 2014016@cau.edu.cn; wangziyu@pku.edu.cn

ORCID: Xinyue Wang: 0000-0002-6428-1361

Author Contributions

Xinyue Wang and Jintong Lin proposed the research project. Xinyue Wang and Ziyu Wang performed the experimentations. Xinyue Wang and Ziyu Wang developed the theoretical model and carried out the analysis. Wen Sun and Rui Liu performed the simulations with the help of Zhongwei Tan. Xinyue Wang and Ziyu Wang wrote the manuscript.

Notes

The authors declare no competing financial interest.

ACKNOWLEDGMENT

This research was supported by the National Natural Science Foundation of China (61605241), and the State Key Laboratory of Advanced Optical Communication Systems and Networks, China (2020GZKF003, 2019GZKF1). The authors thank Zhiyong Zhang and Min Gao for the assistance of sample fabrication, and thank Freya Thomas and Zhiyong Zhang for helpful discussions.

REFERENCES

1. Hess, O.; Pendry, J. B.; Maier, S. A.; Oulton, R. F.; Hamm, J. M.; Tsakmakidis, K. L. Active Nanoplasmonic Metamaterials. *Nat. Mater.* **2012**, 11, 573-584.

2. Chen, H.; Su, L.; Jiang, M.; Fang, X. Highly Desirable Photodetectors Derived from Versatile Plasmonic Nanostructures. *Adv. Funct. Mater*. **2017**, 27, 1704181.

3. Zhao, Z.-J.; Lee, M.; Kang, H.; Hwang, S.; Jeon, S.; Park, N.; Park, S.-H.; Jeong, J.-H. Eight Inch Wafer-Scale Flexible Polarization-Dependent Color Filters with Ag-TiO_2 Composite Nanowires. *ACS Appl. Mater. Interfaces* **2018**, 10, 9188-9196.

4. Zhao, Z.-J.; Shin, S.-H.; Choi, D.-G.; Park, S.-H.; Jeong, J.-H. Shape-Controlled 3D Periodic Metal Nanostructures Fabricated via Nanowelding. *Small* **2018**, 14, 1703102.

5. Sukham, J.; Takayama, O.; Lavrinenko, A. V.; Malureanu, R. High-Quality Ultrathin Gold Layers With an APTMS Adhesion for Optimal Performance of Surface Plasmon Polariton-Based Devices. *ACS Appl. Mater. Interfaces* **2017**, 9, 25049-25056.

6. Wei, C.; Zhao, Y. S. Photonic Applications of Metal-Dielectric Heterostructured Nanomaterials. *ACS Appl. Mater. Interfaces* **2016**, 8, 3703-3713.

7. Wang, W.; Watkins, N.; Yang, A.; Schaller, R. D.; Schatz, G. C.; Odom, T. W. Ultrafast Dynamics of Lattice Plasmon Lasers. *J. Phys. Chem. Lett.* **2019**, 10, 3301-3306.

8. Fernández-Domínguez, A. I.; García-Vidal, F. J.; Martín-Moreno, L. Unrelenting Plasmons. *Nat. Photonics* **2017**, 11, 8-10.

9. Klein, M.; Badada, B.H.; Binder, R.; Alfrey, A.; McKie, M.; Koehler, M. R.; Mandrus, D. G.; Taniguchi, T.; Watanabe, K.; LeRoy, B. J.; Schaibley, J. R. 2D Semiconductor Nonlinear Plasmonic Modulators. *Nat. Commun.* **2019**, 10, 3264.

10. Dai, Y.; Dąbrowski, M.; Apkarian, V. A.; Petek, H. Ultrafast Microscopy of Spin-Momentum-

Locked Surface Plasmon Polaritons. *ACS Nano* **2018**, 12, 6588-6596.

11. Sidiropoulos, T. P. H.; Roder, R.; Geburt, S.; Hess, O.; Maier, S. A.; Ronning, C.; Oulton, R. F. Ultrafast Plasmonic Nanowire Lasers Near the Surface Plasmon Frequency. *Nat. Phys.* **2014**, 10, 870-876.
12. Siddique, R. H.; Kumar, S.; Narasimhan, V.; Kwon, H.; Choo, H. Aluminum Metasurface with Hybrid Multipolar Plasmons for 1000-Fold Broadband Visible Fluorescence Enhancement and Multiplexed Biosensing. *ACS Nano* **2019**, 13, 13775-13783.
13. Wu, T.; Shao, Y.; Wang, Y.; Cao, S. Q.; Cao, W. P.; Zhang, F.; Liao, C. R.; He, J.; Huang, Y. J.; Hou, M. X.; Wang, Y. P. Surface Plasmon Resonance Biosensor Based on Gold-Coated Side-Polished Hexagonal Structure Photonic Crystal Fiber. *Opt. Express* **2017**, 25, 20313-20322.
14. Daems, D.; Pfeifer, W.; Rutten, I.; Saccà, B.; Spasic, D.; Lammertyn, J. Three-Dimensional DNA Origami as Programmable Anchoring Points for Bioreceptors in Fiber Optic Surface Plasmon Resonance Biosensing. *ACS Appl. Mater. Interfaces* **2018**, 10, 23539-23547.
15. Liu, Y.; Yang, C.; Li, H. Cost-Effective and Spectrum-Efficient Coherent OFDM-PON Aided by the Blind ICI Suppression. *IEEE Photonic. Tech. L.* **2015**, 27, 887-890.
16. Hecht, E. *Optics*; Pearson Education: Essex, U.K., **2017**, 338-392.
17. Lan, J.; Yu, W.; Xiao, J. Antiferromagnetic Domain Wall as Spin Wave Polarizer and Retarder. *Nat. Commun.* **2017**, 8, 178.
18. Barnes, W. L.; Dereux, A.; Ebbesen, T. W. Surface Plasmon Subwavelength Optics. *Nature* **2003**, 424, 825-830.
19. Yang, J.; Almossalami, H. A.; Wang, Z.; Wu, K.; Wang, C.; Sun, K.; Yang, Y. M.; Ye, H. Direct Observations of Surface Plasmon Polaritons in Highly Conductive Organic Thin Film. *ACS*

Appl. Mater. Interfaces **2019**, 11, 39132-39142.

20. Birr, T.; Fischer, T.; Evlyukhin, A. B.; Zywietz, U.; Chichkov, B. N.; Reinhardt, C. Phase-Resolved Observation of the Gouy Phase Shift of Surface Plasmon Polaritons. *ACS Photonics* **2017**, 4, 905-908.
21. Maniyara, R. A.; Rodrigo, D.; Yu, R.; Canet-Ferrer, J.; Ghosh, D. S. R.; Yongsunthon, R.; Baker, D. E.; Rezikyan, A.; García de Abajo, F. J.; Pruneri, V. Tunable Plasmons in Ultrathin Metal Films. *Nat. Photonics* **2019**, 13, 328-333.
22. Jung, I.; Kim, M.; Kwak, M.; Kim, G.; Jang, M.; Kim, S. M.; Park, D. J.; Park, S. Surface Plasmon Resonance Extension Through Two-Block Metal-Conducting Polymer Nanorods. *Nat. Commun.* **2018**, 9, 1010.
23. Lin, J.; Mueller, J. P. B.; Wang, Q.; Yuan, G. H.; Antoniou, N.; Yuan, X. C.; Capasso, F. Polarization-Controlled Tunable Directional Coupling of Surface Plasmon Polaritons. *Science* **2013**, 340, 331-334.
24. Kerelsky, A.; Nipane, A.; Edelberg, D.; Wang, D.; Zhou, X.; Motmaendadgar, A.; Gao, H.; Xie, S.; Kang, K.; Park, J.; Teherani, J.; Pasupathy, A. Absence of a Band Gap at the Interface of a Metal and Highly Doped Monolayer MoS_2. *Nano Lett*. **2017**, 17, 5962-5968.
25. Zhang, M.; Magagnosc, D. J.; Liberal, I.; Yu, Y.; Yun, H.; Yang, H.; Wu, Y.; Guo, J.; Chen, W.; Shin, Y. J.; Stein, A.; Kikkawa, J. M.; Engheta, N.; Gianola, D. S.; Murray, C. B.; Kagan, C. R. High-Strength Magnetically Switchable Plasmonic Nanorods Assembled From a Binary Nanocrystal Mixture. *Nat. Nanotechnol.* **2016**, 12, 228-232.
26. Weng, S. J.; Pei, L.; Wang, J. S.; Ning, T. G.; Li, J. High Sensitivity D-Shaped Hole Fiber Temperature Sensor Based on Surface Plasmon Resonance with Liquid Filling. *Photonics Res.* **2017**, 5, 103-107.

27. Wang, X.; Wang, Z. Self-Aligning Polarization Strategy for Making Side Polished Polarization Maintaining Fiber Devices. *Opt. Express* **2010**, 18, 49-55.

28. Hu, W. B.; Ding, L. K.; Zhu, C.; Guo, D. L.; Yuan, Y. Q.; Ma, N.; Chen, W. Optical Fiber Polarizer with Fe-C Film for Corrosion Monitoring. *IEEE Sens. J.* **2017**, 17, 6904-6910.

29. Dong, C. H.; Zou, C. L.; Ren, X. F.; Guo, G. C.; Sun, F. W. In-Line High Efficient Fiber Polarizer Based on Surface Plasmon. *Appl. Phys. Lett.* **2012**, 100, 041104.

30. Azzam, S. I.; Obayya, S. S. A. Titanium Nitride-Based CMOS-Compatible TE-Pass and TM-Pass Plasmonic Polarizers. *IEEE Photonic. Tech. L.* **2016**, 28, 367-370.

31. Bao, Q. L.; Zhang, H.; Wang, B.; Ni, Z. H.; Lim, C. H. Y. X.; Wang, Y.; Tang, D. Y.; Loh, K. P. Broadband Graphene Polarizer. *Nat. Photonics* **2011**, 5, 411-415.

32. Guan, C.; Li, S.; Shen, Y.; Yuan, T.; Yang, J.; Yuan, L. Graphene-Coated Surface Core Fiber Polarizer. *J. Lightwave Technol.* **2015**, 33, 349-353.

33. Li, W. X.; Yi, L. L.; Zheng, R.; Ni, Z. H.; Hu, W. S. Fabrication and Application of a Graphene Polarizer with Strong Saturable Absorption. *Photonics Res.* **2016**, 4, 41-44.

34. Hu, D. J. J.; Ho, H. P. Recent Advances in Plasmonic Photonic Crystal Fibers: Design, Fabrication and Applications. *Adv. Opt. Photonics* **2017**, 9, 257-314.

35. Lee, H. W.; Schmidt, M. A.; Russell, P. St. J. Excitation of a Nanowire “Molecule” in Gold-Filled Photonic Crystal Fiber. *Opt. Lett.* **2012**, 37, 2946-2948.

36. Jo, K.; Song, G. H.; Paek, U. C.; Han, W. T. Fabrication and Polarising Characteristics of D-Shaped Optical Fiber Coated with Chromium Film. *Electron. Lett.* **2001**, 37, 620-621.

37. Dyott, R. B.; Bello, J.; Handerek, V. A. Indium-Coated D-Shaped-Fiber Polarizer. *Opt. Lett.* **1987**, 12, 287-289.

38. Johnstone, W.; Stewart, G.; Hart, T.; Culshaw, B. Surface-Plasmon Polaritions in Thin Metal-

Films and Their Role in Fiber Optic Polarizing Devices. J. *Lightwave Technol*. **1990**, 8, 538-544.

39. Feth, J. R.; Chang, C. L. Metal-Clad Fiber-Optic Cutoff Polarizer. *Opt. Lett.* **1986**, 11, 386-388.

40. Eickhoff, W. In-Line Fiber-Optic Polarizer. *Electron. Lett.* **1980**, 16, 762-763.

41. Okamoto, K. *Fundamentals of Optical Waveguides*; Elsevier Academic Press: Burlington, U.S.A., **2006**, 13-43.

42. Hu, J.; Menyuk, C. R. Understanding Leaky Modes: Slab Waveguide Revisited. *Adv. Opt. Photonics* **2009**, 1, 58-106.

43. Kress, S. J. P.; Antolinez, F. V.; Richner, P.; Jayanti, S. V.; Kim, D. K.; Prins, F.; Riedinger, A.; Fischer, M. P. C.; Meyer, S.; McPeak, K. M.; Poulikakos, D.; Norris, D. J. Wedge Waveguides and Resonators for Quantum Plasmonics. *Nano Lett.* **2015**, 15, 6267-6275.

44. Haffner, C.; Chelladurai, D.; Fedoryshyn, Y.; Josten, A.; Baeuerle, B.; Heni, W.; Watanabe, T.; Cui, T.; Cheng, B.; Saha, S.; Elder, D. L.; Dalton, L. R.; Boltasseva, A.; Shalaev, V. M.; Kinsey, N.; Leuthold, J. Low-Loss Plasmon-Assisted Electro-Optic Modulator. *Nature* **2018**, 556, 7702.

45. Xiong, W.; Hsu, C. W.; Bromberg, Y.; Antonio-Lopez, J. E.; Correa, R. A.; Cao, H. Complete Polarization Control in Multimode Fibers with Polarization and Mode Coupling. *Light-Sci. Appl.* **2018**, 7, 54.

Table of Contents (TOC) graphic